

# A study on the optical properties and optoelectronic parameters of Sudan dye doped poly(5-hydroxy-L-tryptophane) and P(TER-CO-TRI) polymers

Barham K. Rahim<sup>1</sup>, Fahmi F. Muhammadsharif<sup>2</sup>, Salah R. Saeed<sup>3</sup>, Kamal A. Ketuly<sup>4</sup>

<sup>1</sup> Medical Physics Department, Faculty of Medicals & Applied Science, Charho University, Chamchamal 46023, Kurdistan Region, Sulaimania, Iraq

<sup>2</sup> Department of Physics, Faculty of Science and Health, Koya University, Koya 44023, Kurdistan Region-F.R., Iraq

<sup>3</sup> Advanced Polymeric Materials Research Lab., Department of Physics, College of Science, University of Sulaimani, Qlyasan Str., Sulaimani 46001, Iraq

<sup>4</sup> Department of Medical Chemistry, College of Medicine, University of Duhok, 38 Zakho Str., Duhok 1006, Kurdistan Region, Iraq

Corresponding author: Fahmi F. Muhammadsharif (fahmi982@gmail.com)

Received 11 August 2022 ♦ Accepted 3 October 2022 ♦ Published 14 October 2022

**Citation:** Rahim BK, Muhammadsharif FF, Saeed SR, Ketuly KA (2022) A study on the optical properties and optoelectronic parameters of Sudan dye doped poly(5-hydroxy-L-tryptophane) and P(TER-CO-TRI) polymers. *Modern Electronic Materials* 8(3): 85–96. <https://doi.org/10.3897/j.moem.8.3.91521>

## Abstract

In this paper, the optical properties and optoelectronic parameters of two newly synthesized polymers forming a donor : acceptor (D:A) binary system are investigated, followed by their subsequent doping with Sudan dye to obtain a ternary system. The donor polymer is P(TER-CO-TRI), while the acceptor is poly(5-hydroxy-L-Tryptophane). A cost-effective solution-processing was carried out to obtain different binary and ternary composites with concentration of 0.5 mg/ml. Optical absorption spectroscopy was used to measure the optical response and optoelectronic parameters, while FTIR and cyclic voltammetry were used to assess the structure and molecular energy levels of the polymers. The results revealed that the non-dispersive refractive index and energy gap of binary D:A was decreased from 1.56 to 1.52 eV and from 2.84 to 2.10 eV, respectively, when it was doped with Sudan dye. It was concluded that with the help of doping process, different values of energy band gap, refractive index, dielectric constant, and optical conductivity are achieved. This tuning achievement of the optoelectronic parameters is crucial in determining the possible applications of these materials in the organic electronics, photodiodes and photovoltaic devices.

## Keywords

poly(5-hydroxy-L-Tryptophane), P(TER-CO-TRI), sudan dye, energy band gap, extinction coefficient, refractive index, dielectric constant, optical conductivity

## 1. Introduction

The study of optoelectronic parameters and physical properties of organic composites for possible applications in electronic and solution-processed optoelectronic devices has aroused tremendous research interest in recent years. This is primarily due to the low cost and flexibility of organic materials along with the low-temperature and large-scale production capabilities of these materials [1]. For instance, organic semiconductors have contributed to major advances in solution-processed optoelectronic devices [2] perovskite solar cells (PSCs) [3], light-emitting diodes (LEDs) [4], and photodetectors (PDs) [5].

The efficiency of organic solar cells (OSCs) has been steadily improved over the past decade. Recently, a power conversion efficiency (PCE) of over 16% has been obtained in the single-junction OSCs [6].

The organic materials are currently attracting a considerable interest when it comes to the development of organic electronic devices such as transistors, sensors, memory, diodes and solar cells [7–10]. This is due to its one-of-a-kind feature set that enables the creation of lightweight, flexible, easily processable, and cost-effective devices for real-world applications [11, 12].

In the context of photovoltaic and photocatalysis activities, the interaction of light with materials, which allows photons to be absorbed at different energy levels, has become increasingly significant [13–15]. When subjected to photonic radiations, photodiodes are *p-n* junction devices that can generate an electrical signal via the photovoltaic effect. Photodiodes are widely used in a variety of applications, including health care, environmental monitoring, and data transmission [16, 17]. Conventional photodiodes are operated in reverse-biased mode, which means that a negative voltage is applied to the photodiode's positive terminal and vice versa. When a photodiode is exposed to light energy, it produces more free charge carriers, which contributes to the reverse current that flows through the device and being transferred to an external load. Because of their high photonic response, superior stability, and low binding energy of excitons (bounded electron-hole pair), inorganic semiconductors are used in the majority of photodiodes [18–20].

Thiophene-based materials have long been considered among the most promising organic semiconductors for application as active layers in the OSCs [21–24]. The ability of OSC active layers to absorb the largest possible range of the visible spectrum is the most important prerequisite [25]. As such, organic materials showing narrow optical band gap [26] close resemblances to visible light are quite important. The ability to design the electrical and optical response of thiophene rings by replacing hydrogen atoms with certain chemical groups has been confirmed [27].

The contribution of organic materials has been well acknowledged in the application of electronic devices [28–32]. Organic materials are well known

for possessing some important qualities that are rarely seen in the inorganic materials, e.g. high absorption coefficient, optical selectivity, light weight, flexibility, and optoelectronics tuneability [33–36]. To create a more balanced charge carrier among the thin solid films, it is common practice in device manufacturing to mix electron transporting material with hole transporting material in a blend to form a bulk heterojunction active organic layer [37]. A simple solution-processed approach can be used to make a bulk heterojunction active thin film. For a cost-effective production process, this technology is ideal. For tiny organic compounds, numerous researchers have used the physical vapor deposition approach of thin-film creation [38–40].

Because of the significant characteristics of soft organic semiconductors such as low weight, absorption strength, tuneability, and solution-processability with common chemical solvents, the development of organic-based photodiodes or photodetectors has gotten a lot of interest [41–43]. Stretchable organic optoelectronics is currently a promising technique for creating user-friendly integrated electronic systems comprising a variety of functional devices like thin-film transistors (TFTs), LEDs, photodetectors, and photovoltaics. Meanwhile, ongoing research on human-skin and tissue-compatible optoelectronic devices has hinted at their potential in biomedical applications. Continuous, dependable, and accurate monitoring of physiological variables, for example, permits patients to be as mobile as they want without being restricted by their location. Patients can receive real-time self-treatment at home without any constraints on their regular activities by simply transferring the extracted medical data to certified professionals for diagnostic assessment [44]. Therefore, the use of organic semiconductors and dyes has become widespread in electronic devices.

However, to explore the full potential of organic materials and their viability for different emerging applications, a comprehensive study on their optoelectronic parameters, and photo-physical response is necessary. Therefore, the current research paper was devoted to investigate the absorption response, optical energy gap, refractive index, dielectric constant, and optical conductivity of organic composite system made from synthesized electron donating and electron accepting polymers doped with organic dyes.

## 2. Materials and methods

The host polymers of poly(5-hydroxy-L-Tryptophane) behaves like an electron acceptor and P(TER-CO-TRI) presents an electron donor whose molecular structure shown in Fig. 1. The organic materials were used to prepare composite systems without additional purification. The organic materials, poly(5-hydroxy-L-Tryptophane) and P(TER-CO-TRI) were put inside separate vials and dissolved in chloroform solvent following their stirring

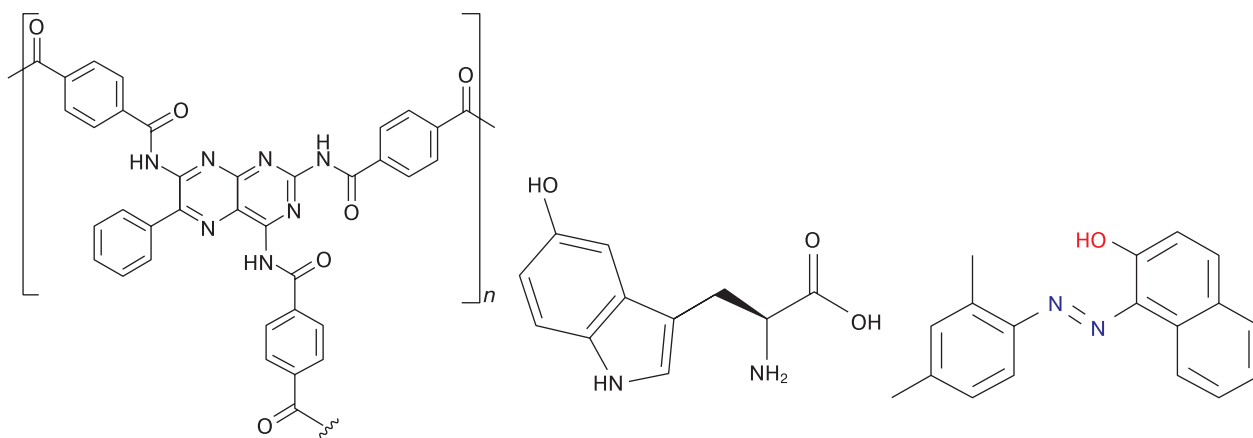


**Figure 1.** Molecular structure of poly(triamterene-co-terephthalate), poly(5-hydroxy-L-Tryptophane) and Sudan dye (from left to right)

overnight using magnetic stirrer. As such, solutions of poly(5-hydroxy-L-Tryptophane) and P(TER-CO-TRI) were formed with concentration of 0.5 mg/ml. Then, different volumetric compositions of Donor : Acceptor (**D : A**) were prepared by mixing the polymer(5-hydroxy-L-Tryptophane) solution with P(TER-CO-TRI) solution with ratios of 1 : 1, 1 : 2, 1 : 3, 1 : 4 and 1 : 5, respectively. Sudan dye was also used to form a ternary composite system. The dye was purchased from Sigma-Aldrich and used as received. Area under the curve of absorption was determined for all ratios of the mixed **D : A**, by which the optimum condition was found to be for the ratio of 1 : 2. Hence, the optoelectronic parameters of the composite at this ratio were comprehensively investigated. The optimized system was then doped by Sudan dye to a ternary system with different ratios of the dye as follows 1 : 2 : 1, 1 : 2 : 2, 1 : 2 : 3, 1 : 2 : 4 and 1 : 2 : 5.

### 3. Results and discussion

#### 3.1. Spectroscopic analysis of P(TRI-CO-TER) and poly (5-hydroxy-L-Tryptophane)

Fourier transformation infrared (**FTIR**) spectroscopy was applied to perform the vibrational analysis of the polymers. FTIR spectra can be used to reveal the molecular structure and molecular environment due to vibrational modes [45]. Figs 2 and 3 show the FTIR spectra for P(TRI-CO-TER) and poly (5-hydroxy-L-Tryptophane) with the main IR characteristic modes, respectively. The absorption bands around 1200 to 1500  $\text{cm}^{-1}$  are assigned to C–H stretching for the aromatic rings and N–H stretching for normal vibration of the pyrrole rings, respectively [46, 47]. In addition, these bands are broad and weak for P(TRI-CO-TER). The reason for this may be that the intensity of the absorption band depends on the magnitude of the change in the dipole moment associated with the vibrations and on the number of bonds responsible for the absorption. Moreover, the formation of cyclic dimers due

to the presence of the carboxylic group, which consists of a proton donor and a proton acceptor group, can lead to the presence of an intermolecular hydrogen bond of the carboxylic acid with pyridine and an intramolecular hy-

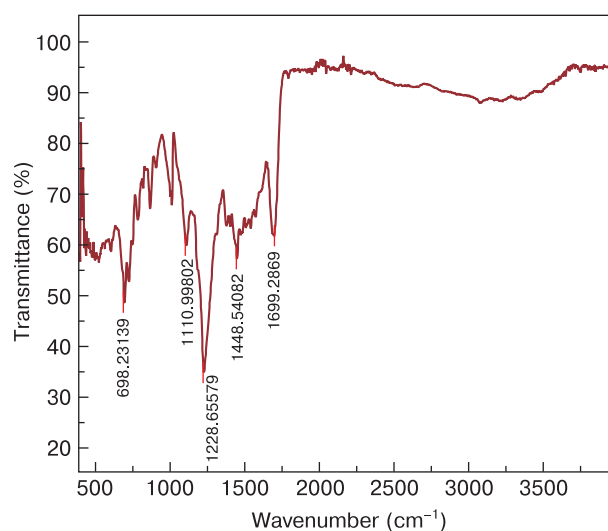


**Figure 2.** FTIR spectra for the P(TRI-co-TER)

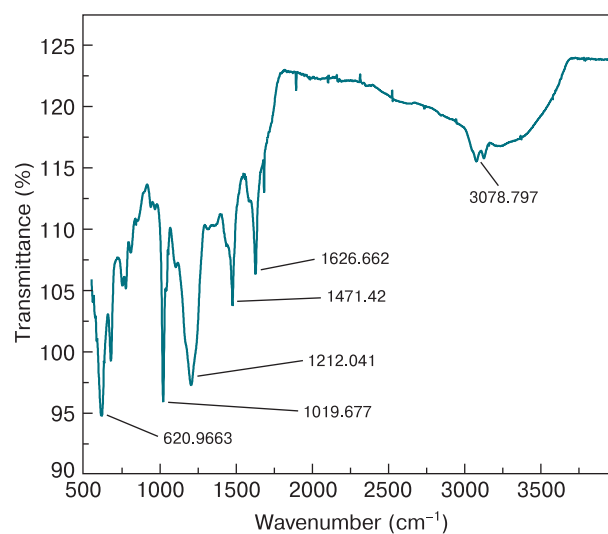


**Figure 3.** FTIR spectra for the poly (5-hydroxy-L-Tryptophane)

drogen bond of the proton donor N–H with oxygen [45]. The band at  $1700\text{ cm}^{-1}$  was attributed to the stretching vibration of the carboxylic group C=O. The out-of-plane bending mode for C—H within the spectral region between  $700$  and  $1000\text{ cm}^{-1}$  could be due to the benzene ring as a result of the polymerisation process [48].

### 3.2. Optical and electrochemical properties

UV–VIS absorption spectroscopy was used to evaluate the photophysical properties of the two newly synthesized polymers. The polymer solution was prepared by dissolving  $0.5\text{ mg}$  of each polymer in  $1\text{ ml}$  of dimethyl sulfoxide (**DMSO**). As known from literary sources, the absorption bands in the UV region can be ascribed to the  $\pi\text{-}\pi^*$  and  $n\text{-}\pi^*$  transitions of delocalized excitons in the polymer chain, whereas the absorption bands in the visible range are assigned to intramolecular charge transfer (**ICT**) between electron-rich moieties and electron-deficient moieties in the main chain [49]. The absorption coefficient spectra (Fig. 4 *a* and *b*) of the polymers were determined using the following equation [50]:

$$\alpha = \frac{2.303A}{t} \quad (1)$$

where  $t$  is the thickness of the cuvette ( $1\text{ cm}$ ) and  $A$  is the absorbance. All two polymers exhibited a sharp absorption band in the UV region which extended to the visible region. The absorption band for Acceptor poly(5-hydroxy-L-Tryptophane) was prolonged until  $419\text{ nm}$  and the absorption band for P(TRI-co-TER) continued until  $438\text{ nm}$ , whereas the absorption band for mixed continued till  $430\text{ nm}$ . This is where the absorption band for the ternary system of D : A: sudan dye expanded to  $580\text{ nm}$ . These indicate that the delocalized excitons' transition from  $\pi\text{-}\pi^*$  and  $n\text{-}\pi^*$  take place in the polymer backbones for the polymers, whereas the differences of prolonged band in the visible region for the polymers is due to the degree of intramolecular charge transfer (**ICT**), which is

related to the transition of excitons between benzenoid and quinoid rings [51].

### 3.3. Optical energy gap and transition types

In optoelectronic applications, it is imperative to have the measurement of the optical energy gap and the type of optical transitions in the conjugated polymers when considering the potential application of the polymers. From the absorption spectra, the optical energy gap and optical transition can be found using Tauc's equation. Furthermore, the absorption edge from the absorption spectrum has been used to determine the optical energy gap, thereby measuring  $\lambda_{\text{onset}}$  as follows [52]:

$$E_g = \frac{1242}{\lambda_{\text{onset}}} \quad (2)$$

However, Tauc's equations can be applied directly to describe the nature of the transition, despite measuring the optical energy gap, i.e. by taking the natural logarithm and deriving Eq. 3,

$$ahv = \alpha_0(hv - E_g)^n, \quad (3)$$

$$\frac{d \ln(\alpha hv)}{d(hv)} = \frac{n}{hv - E_g}, \quad (4)$$

where  $E_g$  is the energy gap,  $\alpha_0$  is the energy-independent constant,  $h$  is the Planck's constant,  $v$  is the frequency of the incident wave, and the value of  $n$  determines the type and nature of the transitions [53]. If the value of  $n = 2$ , the transition is an indirectly allowed transition,  $n = 3$  for indirectly forbidden transitions,  $n = 1/2$  for directly allowed transitions and  $n = 3/2$  for directly forbidden transitions. Figure 5 (*a–d*) shows the absorption onset of the polymers and their equivalent optical energy gaps which were calculated from  $\lambda_{\text{onset}}$  (Eq. 2) and are provided in Table 1. The plots of  $d \ln(\alpha hv)/d(hv)$  versus  $h\nu$  for all samples are shown in Fig. 5 (*f*) and the approximate value

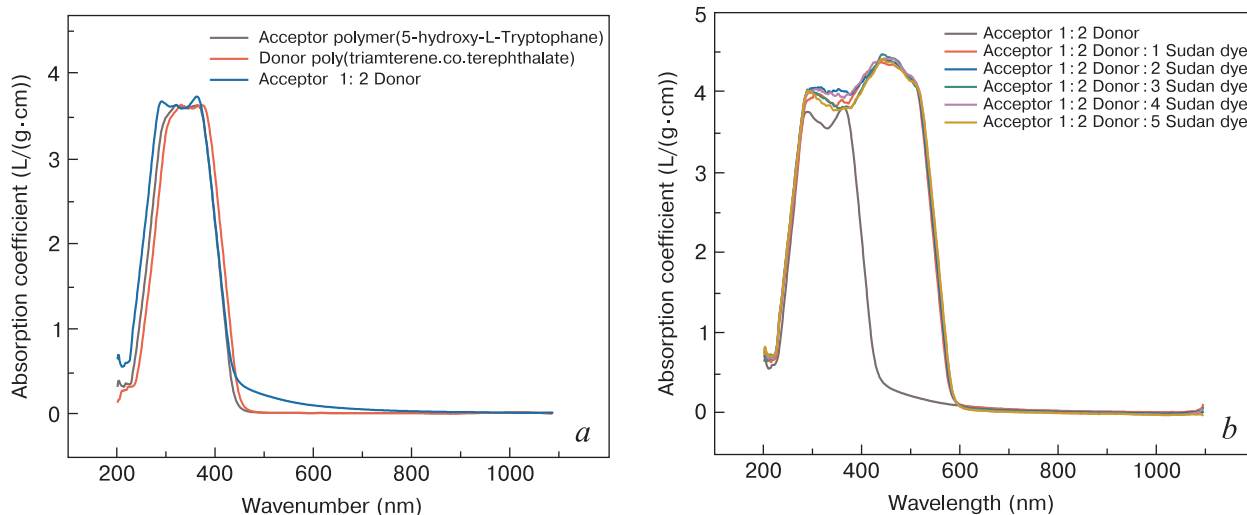


**Figure 4.** Absorption coefficient spectra for the two synthesized polymers, with the binary (*a*) and ternary composite systems (*b*)

of  $h\nu = E_g$  was taken at the peak value. Hence, the estimated value of  $E_g$  was applied for plotting  $\ln(\alpha h\nu)$  versus  $\ln(h\nu - E_g)$  and the value of  $n$  was determined from the slope of the curves and was found to be  $1/2$ , which indicates the occurrence of a directly allowed transition between the intermolecular energy bands of the polymers.

Then, the accurate values of the energy gaps were determined by Tauc's equation by plotting  $(\alpha h\nu)^2$  as a function of  $(h\nu)$  and taking the extrapolation of the linear portion at  $(\alpha h\nu)^2 = 0$ . The positions of the energy gaps are represented in Fig. 5 (e) for all polymers. Also, the determined values of  $E_g$  are shown in Table 1.

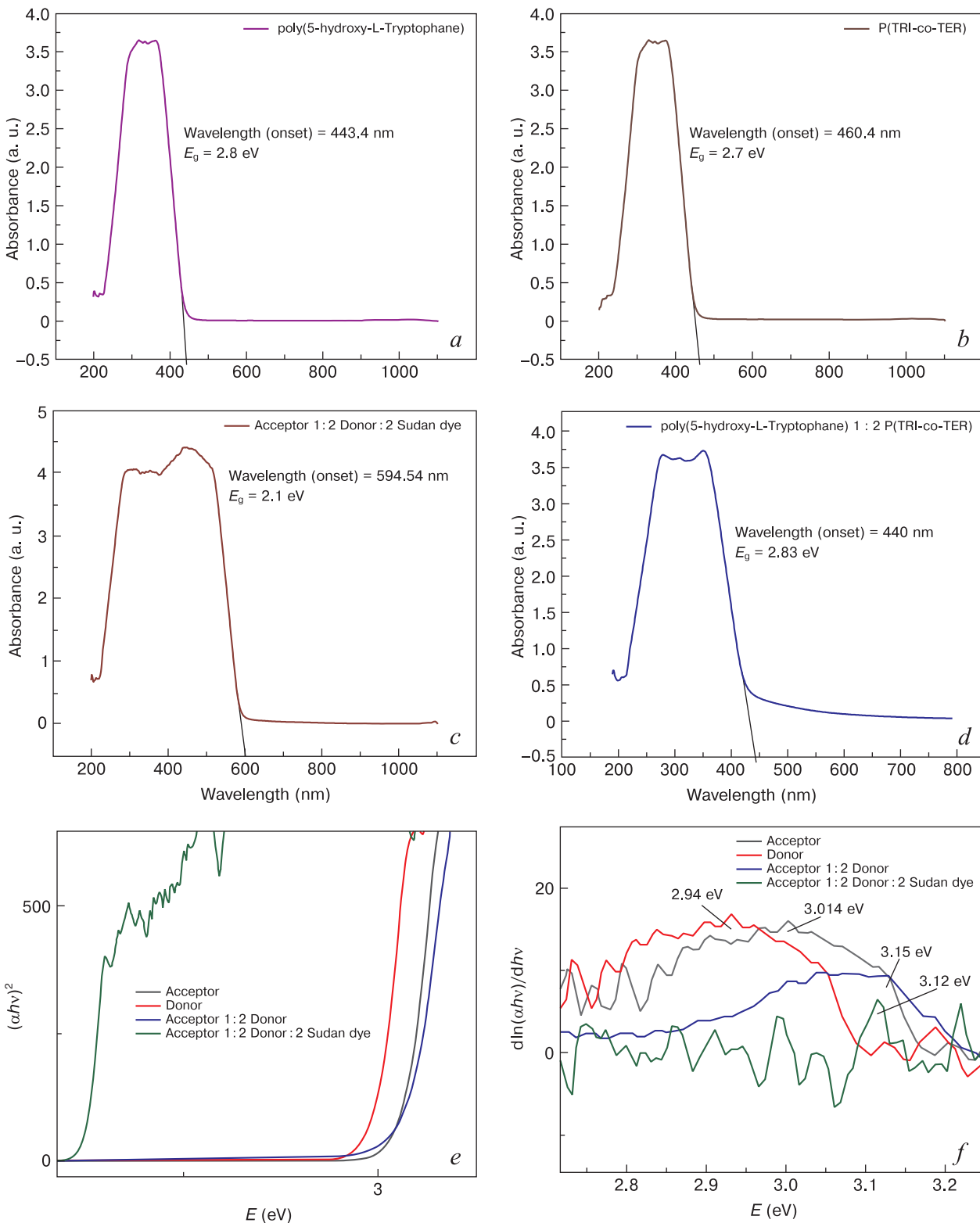


**Figure 5.** Absorbance spectra for all synthesized polymers (a–d), plot of  $(\alpha h\nu)^2$  versus  $E$  for all synthesized polymers (e) and plot of  $d \ln(\alpha h\nu)/d(h\nu)$  versus  $h\nu$  for all synthesized polymers (f)

### 3.4. Electrochemical properties

There are several parameters that should be considered in designing and optimizing organic photovoltaic devices which include charge transfer and charge collection at the active medium and electrodes. In this respect, electrochemical study provides information regarding the position of the HOMO and LUMO levels of organic materials prior to device fabrication. Cyclic voltammetry (CV) constitutes a reliable method for estimating energy levels from the oxidation and reduction potentials for the corresponding materials. The oxidation and reduction potentials are identified from the onset potential, which is defined as the potential where holes or electrons are initially injected into the HOMO and LUMO levels, respectively, and anodic or cathodic current growth becomes evident [54]. To estimate the position of the HOMO and LUMO levels, first, optical energy gaps were estimated from Tauc's equation (Section "Optical energy gap and transition types"). Second, the LUMO and HOMO levels were calculated from the observable reduction and oxidation potentials from CV measurements for all the polymers. Then, the HOMO and LUMO levels were estimated from the relation below using ferrocene as the reference couple [55]:

$$E_{\text{HOMO}} = -(E(\text{onset,ox.Fc}^+/\text{Fc}) + 5.39) \text{ (eV)}, \quad (5)$$

$$E_{\text{LUMO}} = -(E(\text{onset,red.Fc}^+/\text{Fc}) + 5.39) \text{ (eV)}, \quad (6)$$

$$E_{\text{g}}^{\text{Tauc}} = E_{\text{HOMO}} - E_{\text{LUMO}}. \quad (7)$$

**Table 1.** Determined energy gap for synthesized polymers from absorbance data

Materials	$E_{\text{g}}^{\lambda_{\text{onset}}}$ (eV)	$E_{\text{g}}^{\text{Tauc}}$ (eV)
Donor P(TRI-co-TER)	2.70	2.97
Acceptor poly(5-hydroxy-L-Tryptophane)	2.80	2.94
Donor : Acceptor (1 : 2)	2.84	2.97
Donor : Acceptor : Dye (1 : 2 : 2)	2.10	2.22

Illustrative CVs of the two polymers, versus  $\text{Fc}/\text{Fc}^+$ , are presented in Fig. 6, while the corresponding electrochemical parameters are shown in Table 1. The HOMO level is influenced by the type of substituents (whether electron withdrawing or electron donating species) and it can be seen that the polymer P(TRI-co-TER) exhibits a relatively high HOMO level compared to poly(5-hydroxy-L-tryptophan). This could be due to the presence of the indole N-H group. In addition, P(TRI-co-TER) exhibits relatively similar molecular energy levels to that of P3HT, and also the LUMO level of P(TRI-co-TER) is 2.92 eV, but the LUMO level of poly(5-hydroxy-L-Tryptophane) is 3.19 eV (calculated from  $E_{\text{ox}}$  and  $E_{\text{g}}$  due to the weak observation of  $E_{\text{red}}$  on the CV plot) as shown in Table 2 [56].

### 3.5. Optical constants

Optical constants such as refractive index and extinction coefficient, and their derivative parameters like dielectric constant and optical conductivity, should be considered before applying the materials in photovoltaic devices.

**Table 2.** Electrochemical and optical data for the synthesized polymers

Polymer	$E_{\text{onset,ox}}$ (V)	$E_{\text{onset,red}}$ (V)	$E_{\text{HOMO}}$ (eV)	$E_{\text{LUMO}}$ (eV)	$E_{\text{g}}^{\text{opt}}$ (eV)
P(TRIco-TER)	0.31	-1.24	-5.70	-2.78	2.92
poly(5-hydroxy-L-Tryptophane)	0.14	-2.20	-5.53	-3.19	2.34

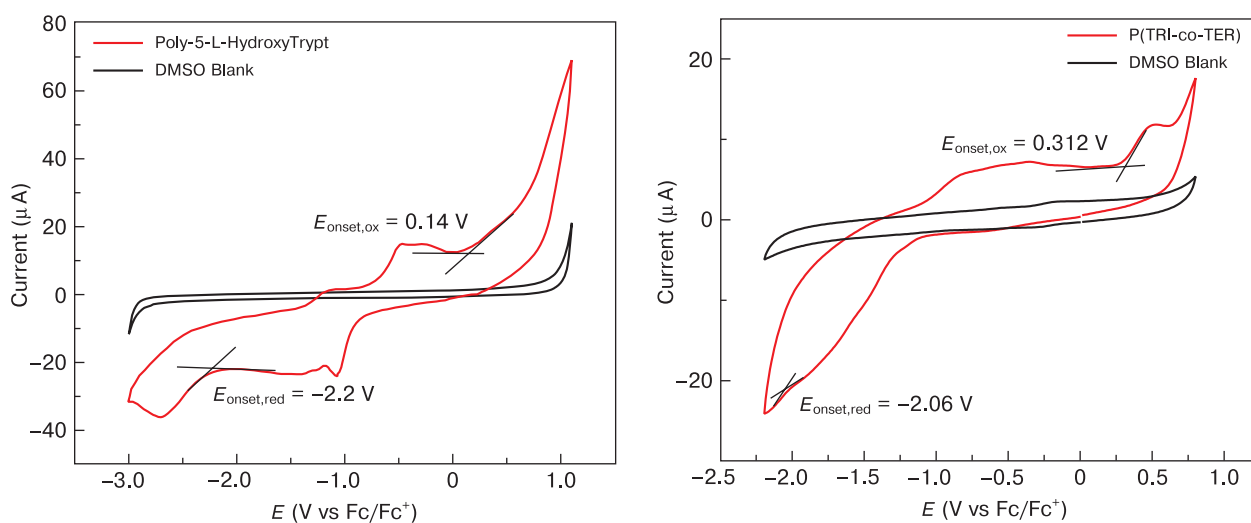


**Figure 6.** The cyclic voltammetry (CV) spectra for the two polymers. The irreversible oxidative processes observed in the CVs are likely due to the oxidation of adventitious water in the DMSO solvent

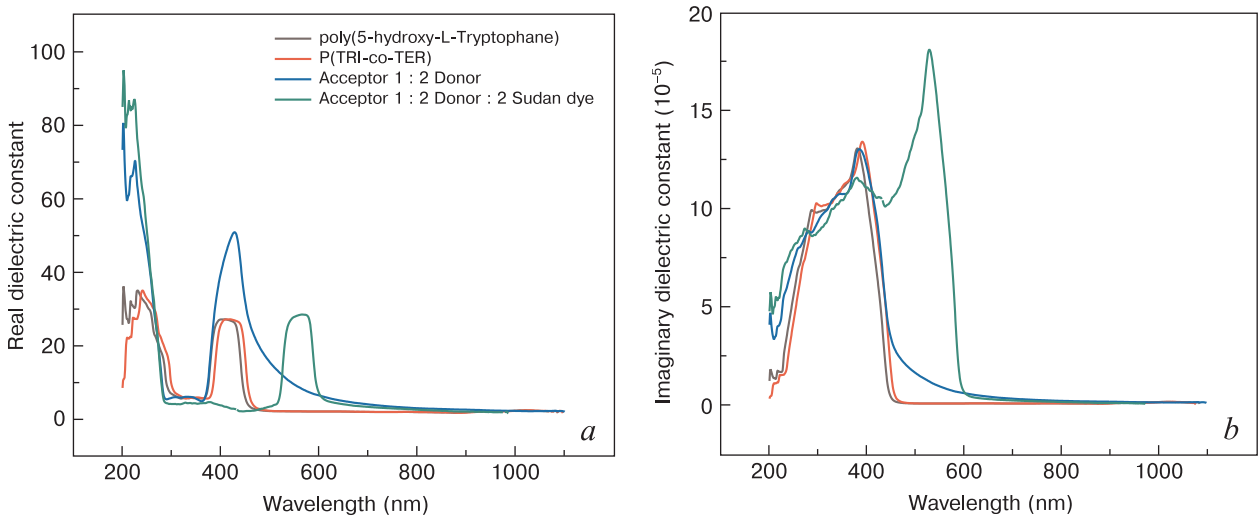


**Figure 7.** Dielectric constant spectra for the synthesized polymers; (a) real part and (b) imaginary part

The way an electromagnetic wave propagates through materials and how the velocity within a material changes with respect to a vacuum is revealed by studying the refractive index. Furthermore, it constitutes a complex variable, the imaginary part of which indicates the amount of energy lost due to the medium, which is referred to as the extinction coefficient. The absorbance data were used to calculate both refractive index ( $n$ ) and extinction coefficient ( $k$ ) using Eqs. 8 and 9 [57].

$$n = \frac{-2(R+1) - \sqrt{4k^2 R^2 + 16R - 4k^2}}{2(R-1)}, \tag{8}$$

$$k = \frac{\alpha\lambda}{4\pi}, \tag{9}$$

where  $\alpha$  is the absorption coefficient and  $R$  is the reflectance. They were calculated using Eq. 4 and the following formula  $R = 1 - T - A$ , where  $A$  is absorbance and  $T$  is transmittance and estimated from  $T = 10^{-A}$ . Figs 8, and 9 show the variation of refractive index and extinction co-

efficient, respectively as a function of wavelength from 200 to 1100 nm. Results show that the P(TRI-co-TER) and poly(5-hydroxy-L-Tryptophane) exhibit a wide dispersion region ranging from 300 to 500 nm and 256 to 423 nm, respectively. For the binary 1 : 2 (A : D) the region is extended from 276 to 402 nm, while for the ternary system (D : A : sudan) the spectrum covers from 253 to 554 nm.

Furthermore, the extinction coefficient ( $k$ ) designates the loss of the incident photon due to scattering and absorption within the medium. Noticeably, the variation of ( $k$ ) is almost comparable to the corresponding absorp-tion coefficient (Eq. 9) [58]. All samples demonstrate a sharp absorption region in the UV range, extending to varying degrees into the visible region.

The optical dielectric constant ( $\epsilon$ ) represents a frequency-dependent parameter and indicates the electronic response to the incident photon in the material. Meanwhile, the dielectric constant is a complex function and its real part is assigned to polarization upon the impact of an electromagnetic field whereas the imaginary

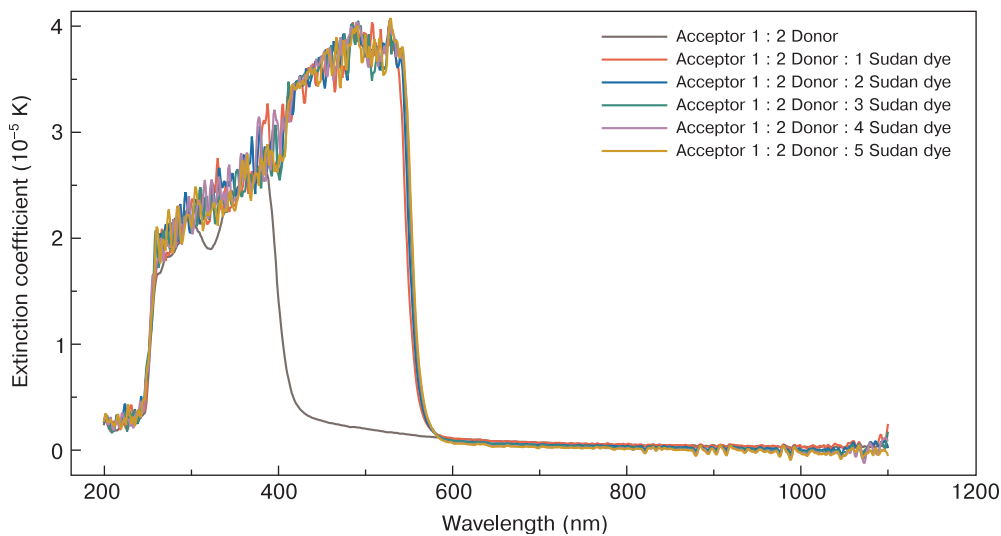


**Figure 8.** The extinction coefficient spectra of the binary and ternary composite systems

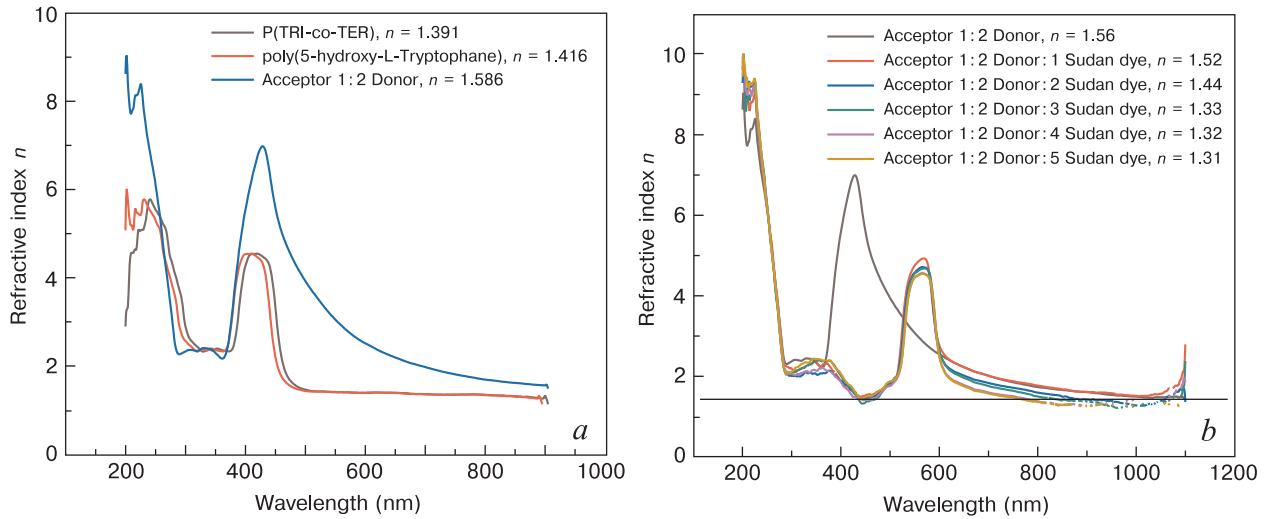


**Figure 9.** Refractive index spectra of the pristine of the donor, acceptor, binary and ternary systems

part represents the optical loss and is described by the following equations [59].

$$\varepsilon = \varepsilon_1 + i\varepsilon_2, \quad (10)$$

$$\varepsilon_1 = n^2 - k^2, \quad (11)$$

$$\varepsilon_2 = 2nk, \quad (12)$$

$$\tan \delta = \frac{\varepsilon_2}{\varepsilon_1}, \quad (13)$$

where  $\varepsilon_1$  represents the real part and  $\varepsilon_2$  represents the imaginary part of the dielectric constant. Fig. 7 (a and b) shows the fluctuation of optical dielectric constant with respect to the wavelength from 200 to 1100 nm. It is noteworthy that the real part of the spectrum of the optical dielectric constant captures the refractive index due to the small value of  $k$ , while the imaginary part is essentially based on the absorption coefficient (see Eqs. 9, 11 and 12). Show that the P(TRI-co-TER) and poly(5-hydroxy-L-Tryptophane), than for this mixed Acceptor 1 : 2 Donor and this mixed Acceptor 1 : 2 Donor : 2 sudan dye.

Fig. 9 shows the refractive index of the studied solution in the wavelength range from 200 to 1000 nm. It was observed that refractive index follows an anomalous dispersion in the UV and near Vis wavelength (absorption region) and a non-dispersive response in the far Vis and IR wavelengths (transparent region). The non-dispersive/flattened property of refractive index is called infinite refractive index ( $n_\infty$ ). Its value for the investigated solution is shown in Table 3. It was revealed that the refractive index of P(TRI-co-TER) ( $n = 1.39$ ) and that the refractive index of poly(5-hydroxy-L-Tryptophane) ( $n = 1.416$ ) are lower than that of the binary system ( $n = 1.586$ ) and lower than that of the ternary composite system ( $n = 1.52$ ), which is consistent with the data presented in the literary sources [60].

Interestingly, with the help of poly(5-hydroxy-L-Tryptophane) ( $n = 1.416$ ) dopant it is possible to increase the

**Table 3.** The studied optoelectronic parameters of the poly(5-hydroxy-L-Tryptophane), P(TRI-co-TER), binary and ternary systems

System	$n$	$\varepsilon_r$	$\sigma_r \cdot 10^{-4}$ (S/cm)
P(TRI-co-TER)	1.390	2.86	2.43
poly(5-hydroxy-L-Tryptophane)	1.416	1.99	3.60
Donor : Acceptor (1 : 2)	1.560	2.86	2.64
Donor : Acceptor : Dye (1 : 2 : 2)	1.520	2.69	2.32

refractive index of P(TRI-co-TER) from ( $n = 1.39$ ) to ( $n = 1.586$ ) than ( $n = 1.52$ ) in the Acceptor : Donor (1 : 2) system (binary) than this Acceptor 1 : 2 Donor : 2 sudan dye system. The refractive index peak shifts to the blue with increasing poly(5-hydroxy-L-tryptophan) content, reflecting the expectation of a corresponding decrease in the energy gap.

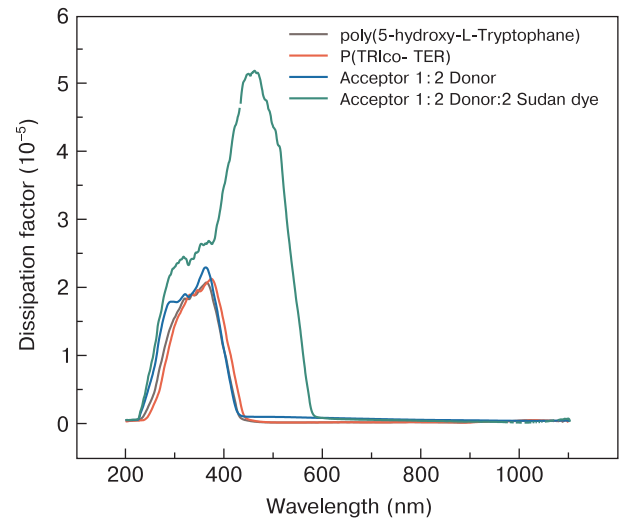


**Figure 10.** Dielectric lost tangent (dissipation factor) spectra for all synthesized polymers

Furthermore, the real and imaginary components of optical conductivity ( $\sigma^* = \sigma_r + i\sigma_i$ ) can be investigated using the following formula:

$$\sigma_r = \omega \varepsilon_0 \varepsilon_i, \quad (14)$$

$$\sigma_i = \omega \varepsilon_0 \varepsilon_r. \quad (15)$$

Where  $\sigma_r$  is the real optical conductivity,  $\sigma_i$  is the imaginary optical conductivity,  $\omega$  is the angular frequency and  $\varepsilon_0$  is free space permittivity ( $8.85 \cdot 10^{-12}$  F/m). Fig. 11 (a) shows the  $\sigma_r$  spectra of the investigated binary and ternary composite systems. One can notice from the figure that the value of real optical conductivity is getting constant/non-dispersive at the high wavelengths. This indicates that the change in optical conductivity is directly related

due to the improved  $\pi$ - $\pi$  stacking and reduced band gap energy.

## 4. Conclusions

A broad spectrum of investigation on the optical properties and optoelectronic parameters of P(TER-CO-TRI), and poly(5-hydroxy-L-Tryptophane) along with their doping with sudan dye was successfully performed. Optical spectroscopy has been found to be extremely effective in measuring the optoelectronic parameters of binary and ternary composites of polymeric materials and dye. It was concluded that with the help of doping process, different values of energy band gap, refractive index, dielectric constant, and optical conductivity are achieved.

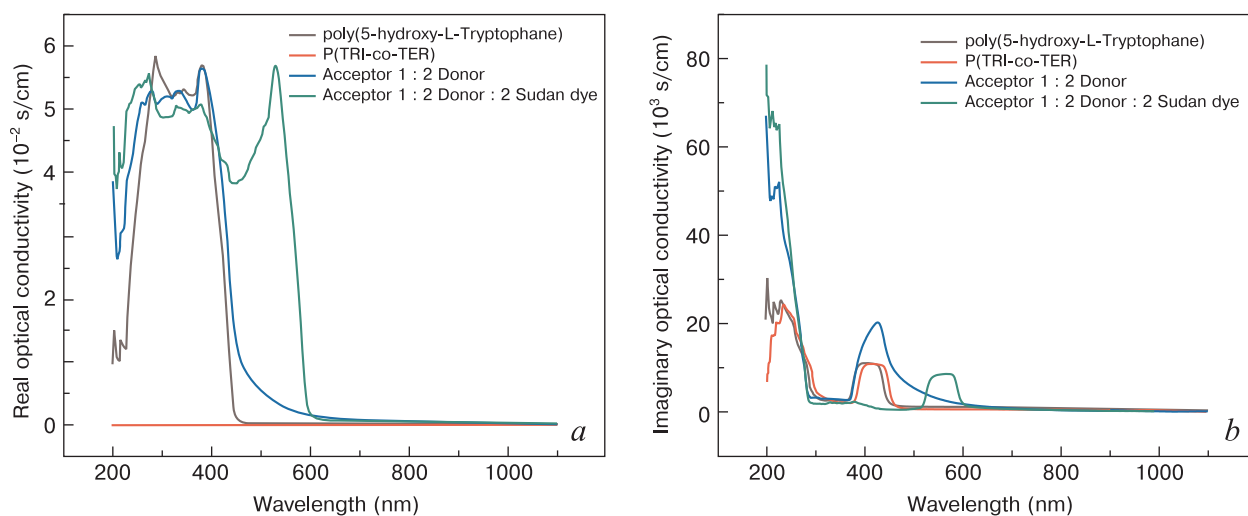


**Figure 11.** Optical conductivity spectra for all synthesized polymers; (a) real part and (b) imaginary part

to the variation of excited electrons due to the absorption of photon energy by the solutions. Therefore, the increment in optical absorption of the studied solutions in the UV region is a consequence of increased optical conductivity and vice versa. Fig. 11 (b) shows the spectra of imaginary optical conductivity for the binary and ternary systems. Results show that  $\sigma_i$  is exponentially decreases with the increase of wavelength. Noticeably, a pronounced decrease in  $\sigma_i$  is resulted by doping the poly(5-hydroxy-L-Tryptophane), especially in the UV spectral region. However, the ternary composite exhibits higher  $\sigma_i$  compared to the other solutions, which may be

This tuning achievement of the optoelectronic parameters is crucial in determining the possible applications of these materials in the organic electronics, photodiodes and photovoltaic devices.

## Acknowledgement

Barham K. Rahim would like to Mr. Peshawa O. Amin for his ongoing support during the experimental setup and data collection process. Kamal A. Ketuly thanks the Erasmus+ scheme for facilitating collaboration between the University of Duhok and the University of Glasgow.

## References

1. Wang F., Tan Z., Li Y. Solution-processable metal oxides/chelates as electrode buffer layers for efficient and stable polymer solar cells. *Energy and Environmental Science*. 2015; 8(4): 1059–1091. <https://doi.org/10.1039/c4ee03802a>
2. You J., Dou L., Yoshimura K., Kato T., Ohya K., Moriarty T., Emery K., Chen C.-C., Gao J., Li G., Yang Y. A polymer tandem solar cell with 10.6% power conversion efficiency. *Nature Communications*. 2013; 4: 1410–1446. <https://doi.org/10.1038/ncomms2411>

3. Zhang H., Nazeeruddin M.K., Choy W.C.H. Perovskite photovoltaics: the significant role of ligands in film formation, passivation, and stability. *Advanced Materials*. 2019; 31(8): e1805702–e1805731. <https://doi.org/10.1002/adma.201805702>
4. Mao J., Sha W., Zhang H., Ren X., Zhuang J., Roy V., Wong K., Choy W. Novel direct nanopatterning approach to fabricate periodically nanostructured perovskite for optoelectronic applications. *Advanced Functional Materials*. 2017; 27(10): 1606525–1606535. <https://doi.org/10.1002/adfm.201606525>
5. Zhu H.L., Liang Z., Huo Z., Ng W.K., Mao J., Wong K., Yin W., Choy W. Low-bandgap methylammonium-rubidium cation Sn-rich perovskites for efficient ultraviolet – visible – near infrared photodetectors. *Advanced Functional Materials*. 2018; 28(16): 1706068–1706077. <https://doi.org/10.1002/adfm.201706068>
6. Fan B., Zhang D., Li M., Zhong W., Zeng Z., Ying L. Achieving over 16% efficiency for single-junction organic solar cells. *Science China Chemistry*. 2019; 64(4): 746–752. <https://doi.org/10.1007/s11426-019-9457-5>
7. Ang Q.Y., Zolkeflay M.H., Low S.C. Applied surface science configuration control on the shape memory stiffness of molecularly imprinted polymer for specific uptake of creatinine. *Applied Surface Science*. 2016; 369: 326–333. <https://doi.org/10.1016/j.apusc.2016.02.076>
8. Jayabharathi J., Thanikachalam V., Ramanathan P. Phenanthrimidazole as a fluorescent sensor with logic gate operations. *Spectrochimica Acta Part A: Molecular and Biomolecular Spectroscopy*. 2015; 150: 886–891. <https://doi.org/10.1016/j.saa.2015.06.044>
9. Lazim H.G., Ajeel K.I., Bdran H.A. The photovoltaic efficiency of the fabrication of copolymer P3HT : PCBM on different thickness nano- anatase titania as solar cell. *Spectrochimica Acta Part A: Molecular and Biomolecular Spectroscopy*. 2015; 145: 598–603. <https://doi.org/10.1016/j.saa.2015.02.096>
10. Sarjidan M.A.M., Basri S.H., Za'aba N.K., Zaini M.S., Majid W.H.A.B.D. Electroluminescence and negative differential resistance studies of TPD : PBD : Alq3 blend organic-light-emitting diodes. *Bulletin of Materials Science*. 2015; 38(1): 235–239. <https://doi.org/10.1007/s12034-014-0807-6>
11. Pagliaro M., Ciriminna R., Palmisano G. Flexible solar cells. *ChemSusChem*. 2008; 1(11): 880–891. <https://doi.org/10.1002/cssc.200800127>
12. Krebs F.C. All solution roll-to-roll processed polymer solar cells free from indium-tin-oxide and vacuum coating steps. *Organic Electronics*. 2009; 10(5): 761–768. <https://doi.org/10.1016/j.orgel.2009.03.009>
13. Zinatloo-ajabshir S., Sadat M., Salavati-niasari M. Eco-friendly synthesis of Nd<sub>2</sub>Sn<sub>2</sub>O-based nanostructure materials using grape juice as green fuel as photocatalyst for the degradation of erythrosine. *Composites Part B. Engineering*. 2019; 167(3): 643–653. <https://doi.org/10.1016/j.compositesb.2019.03.045>
14. Razi F., Zinatloo-ajabshir S., Salavati-niasari M. Preparation, characterization and photocatalytic properties of Ag<sub>2</sub>ZnI<sub>4</sub>/AgI nanocomposites via a new simple hydrothermal approach. *Journal of Molecular Liquids*. 2017; 225: 645–651. <https://doi.org/10.1016/j.molliq.2016.11.028>
15. Zinatloo-ajabshir S., Mortazavi-derazkola S., Salavati-niasari M. Nd<sub>2</sub>O<sub>3</sub>–SiO<sub>2</sub> nanocomposites: A simple sonochemical preparation, characterization and photocatalytic activity. *Ultrasonics Sonochemistry*. 2018; 42: 171–182. <https://doi.org/10.1016/j.ultsonch.2017.11.026>
16. Alzoubi T., Qutaish H., Al-shawwa E., Hamzawy S. Enhanced UV-light detection based on ZnO nanowires / graphene oxide hybrid using cost-effective low temperature hydrothermal process. *Optical Materials*. 2018; 77: 226–232. <https://doi.org/10.1016/j.optmat.2018.01.045>
17. Alamdari S., Ghamsari M.S., Afarideh H., Mohammadi A., Geranmayeh S., Tafreshi M.J., Ehsani M., Majles Ara M.H. Preparation and characterization of GO-ZnO nanocomposite for UV detection application. *Optical Materials*. 2019; 92: 243–250. <https://doi.org/10.1016/j.optmat.2019.04.041>
18. Xu Q., Cheng L., Meng L., Wang Z., Bai S., Tian X., Jia X., Qin Y. Flexible self-powered ZnO film UV sensor with a high response. *ACS Applied Materials and Interfaces*. 2019; 11(29): 26127–26133. <https://doi.org/10.1021/acsami.9b09264>
19. Wang H., Sun P., Cong S., Wu J., Gao L., Wang Y., Dai X., Yi Q., Zou G. Nitrogen-doped carbon dots for 'green' quantum dot solar cells. *Nanoscale Research Letters*. 2016; 11(1): 1–6. <https://doi.org/10.1186/s11671-016-1231-1>
20. Guo D., Su Y., Shi H., Li P., Zhao N., Ye J., Wang S., Liu A., Chen Zh., Li Ch., Tang W. Self-powered ultraviolet photodetector with superhigh photoresponsivity (3.05 A/W) based on the GaN/Sn:Ga<sub>2</sub>O<sub>3</sub> pn Junction. *ACS Nano*. 2018; 12(12): 12827–12835. <https://doi.org/10.1021/acsnano.8b07997>
21. Al-ibrahim M., Sensfuss S., Uziel J., Ecke G., Ambacher O. Comparison of normal and inverse poly (3-hexylthiophene)/fullerene solar cell architectures. *Solar Energy Materials and Solar Cells*. 2005; 85(2): 277–283. <https://doi.org/10.1016/j.solmat.2004.08.001>
22. Baek W., Yang H., Yoon T., Kang C.J. Solar energy materials & solar cells effect of P3HT : PCBM concentration in solvent on performances of organic solar cells. *Solar Energy Materials and Solar Cells*. 2009; 93(8): 1263–1267. <https://doi.org/10.1016/j.solmat.2009.01.019>
23. Chen D., Nakahara A., Wei D., Nordlund. D., Russell T.P. P3HT/PCBM bulk heterojunction organic photovoltaics: correlating efficiency and morphology. *Nano Letters*. 2011; 11(2): 561–567. <https://doi.org/10.1021/nl103482n>
24. Guo T. Effects of film treatment on the performance of organic solar cells. 2008; 516: 3138–3142. <https://doi.org/10.1016/j.tsf.2007.08.066>
25. Kim J.Y., Lee K., Coates N.E., Moses D., Nguyen T.-Q., Dante M., Heeger A.J. Efficient tandem polymer solar cells fabricated by all-solution processing. *Science*. 2007; 317(5835): 222–225. <https://doi.org/10.1126/science.1141711>
26. Colladet K., Fourier S., Cleij T., Lutsen L., Gelan J., Vanderzande D., Nguyen L.H., Neugebauer H., Sariciftci S., Aguirre A., Janssen G., Goovaerts E. Low band gap donor-acceptor conjugated polymers toward organic solar cells applications. *Macromolecules*. 2007; 40(1): 65–72. <https://doi.org/10.1021/MA061760I>
27. Liu X., Knupfer M., Huisman B. Electronic properties of the interface between  $\alpha,\omega$ -dihexyl-quaterthiophene and gold. *Surface Science*. 2005; 595(1-3): 165–171. <https://doi.org/10.1016/j.susc.2005.08.007>
28. Vickers N.J. Animal communication : When I'm calling you, will you answer too? *Current Biology*. 2017; 27(14): R713–R715. <https://doi.org/10.1016/j.cub.2017.05.064>

29. Sharma G., Hashmi S., Kumar U., Kattayat S., Ahmad M.A., Kumar Sh., Dalela S., Alvi P.A. Optical and electronic characteristics of ITO/NPB/Alq<sub>3</sub>:DCJT/Alq<sub>3</sub>/Ag heterostructure based organic light emitting diode. *Optik*. 2020; 223: 165572. <https://doi.org/10.1016/j.ijleo.2020.165572>
30. Fariq F., Sulaiman K. Photovoltaic performance of organic solar cells based on DH6T/PCBM thin film active layers. *Thin Solid Films*. 2011; 519(15): 5230–5233. <https://doi.org/10.1016/j.tsf.2011.01.165>
31. Chenot C., Robiette R., Collin S. First evidence of the cysteine and glutathione conjugates of 3-sulfanylpentan-1-ol in hop (*Humulus lupulus* L.). *Journal of Agricultural and Food Chemistry*. 2019; 67(14): 4002–4010. <https://doi.org/10.1021/acs.jafc.9b00225>
32. Lochner C.M., Khan Y., Pierre A., Arias A.C. All-organic optoelectronic sensor for pulse oximetry. *Nature Communications*. 2014; 5: 5745. <https://doi.org/10.1038/ncomms6745>
33. Sajid M., Zubair M., Hoi Y.D., Na K.-H., Choi K.H. Flexible large area organic light emitting diode fabricated by electrohydrodynamics atomization technique. *Journal of Materials Science: Materials in Electronics*. 2015; 26(9): 7192–7199. <https://doi.org/10.1007/s10854-015-3344-1>
34. Gahungu G., Zhang J. “CH”N Substituted mer-Gaq<sub>3</sub> and mer-Alq<sub>3</sub> derivatives: an effective approach for the tuning of emitting color. *The Journal of Physical Chemistry. B*. 2005; 109(37): 17762–17767. <https://doi.org/10.1021/JP052220A>
35. Kim M.-J., An T., Kim S.-O., Cha H., Kim H.N., Xiofeng T., Park Ch.E., Kim Y.-H. Molecular design and ordering effects of alkoxy aromatic donor in a DPP copolymer on OTFTs and OPVs. *Materials Chemistry and Physics*. 2014; 153: 63–71. <https://doi.org/10.1016/j.matchemphys.2014.12.035>
36. Yang D., Ma D. Development of organic semiconductor photodetectors: from mechanism to applications. *Advanced Optical Materials*. 2018; 7(1): 1800522–1800545. <https://doi.org/10.1002/adom.201800522>
37. Vuuren R.D.J., Armin A., Pandey A.K., Burn P.L., Meredith P. Organic photodiodes: the future of full color detection and image sensing. *Advanced Materials*. 2016; 28(24): 4766–4802. <https://doi.org/10.1002/adma.201505405>
38. Dai Q., Zhang X.Q. High-response ultraviolet photodetector based on N,N-bis(naphthalen-1-yl)-N,N-bis(phenyl)benzidine and 2-(4-tertbutylphenyl)-5-(4-biphenyl)-1,3,4-oxadiazole. *Optics Express*. 2010; 18(11): 11821–11826. <https://doi.org/10.1364/OE.18.011821>
39. Qian D.A.I., Lu Z.H.U., Jian S.U.N., Xiqing Z., Yongsheng W. Organic photodetectors based on transparent electrodes for application in ultraviolet light detection. *Science China Technological Sciences*. 2012; 55(6): 1551–1555. <https://doi.org/10.1007/s11431-012-4806-9>
40. Ray D., Narasimhan K.L. High response organic visible-blind ultraviolet detector. *Applied Physics Letters*. 2007; 91(9): 093516–093520. <https://doi.org/10.1063/1.2778545>
41. Zhang L., Yang T., Shen L., Fang Y., Dang L., Zhou N., Guo X., Hong Z., Yang Y., Wu H., Huang J., Liang Y. Toward highly sensitive polymer photodetectors by molecular engineering. *Advanced Materials*. 2015; 27(41): 6496–6503. <https://doi.org/10.1002/adma.201502267>
42. Omidvar A. Electronic structure tuning and band gap opening of nitrogen and boron doped holey graphene flake: The role of single/dual doping. *Materials Chemistry and Physics*. 2017; 202: 258–265. <https://doi.org/10.1016/j.matchemphys.2017.09.025>
43. Muhammad F.F., Yahya M.Y., Aziz F., Rasheed M.A., Sulaiman K. Tuning the extinction coefficient, refractive index, dielectric constant and optical conductivity of Gaq<sub>3</sub> films for the application of OLED displays technology. *Journal of Materials Science: Materials in Electronics*. 2017; 28: 14777–14786. <https://doi.org/10.1007/s10854-017-7347-y>
44. Lee H., Jiang Z., Yokota T., Fukuda K., Sungjun P., Someya T. Stretchable organic optoelectronic devices: Design of materials, structures, and applications. *Materials Science & Engineering R-reports*. 2021; 146: 100631. <https://doi.org/10.1016/j.mser.2021.100631>
45. Duygu D.Y., Baykal T., Açıkgöz Đ., Yildiz K. Fourier transform infrared (FT-IR) spectroscopy for biological studies. *Gazi University Journal of Science*. 2009; 22(3): 117–121.
46. Świdwerski G., Wojtulewski S., Kalinowska M., Świsłocka R., Lewandowski W. Effect of alkali metal ions on the pyrrole and pyridine  $\pi$ -electron systems in pyrrole-2-carboxylate and pyridine-2-carboxylate molecules: FT-IR, FT-Raman, NMR and theoretical studies. *Journal of Molecular Structure*. 2011; 993: 448–458. <https://doi.org/10.1016/j.molstruc.2011.01.026>
47. Schmidt L.A., Arias R.J.J., Santos B.P.S., Marques M.F.V., Monteiro S.N. Synthesis and characterization of novel conjugated copolymers for application in third generation photovoltaic solar cells. *Journal of Materials Research and Technology*. 2020; 9(4): 7975–7988. <https://doi.org/10.1016/j.jmrt.2020.05.009>
48. Butoi B., Groza A., Dinca P., Bălan A., Barna V. Morphological and structural analysis of polyaniline and poly(o-anisidine) layers generated in a DC glow discharge plasma by using an oblique angle electrode deposition configuration. *Polymers*. 2017; 9: 732–750. <https://doi.org/10.3390/polym9120732>
49. Huang Y., Wu F., Zhang M., Mei S., Shen P., Tan S. Synthesis and photovoltaic properties of conjugated polymers with an asymmetric 4-(2-ethylhexyloxy)-8-(2-ethylhexylthio)benzo[1,2-b:4,5-b'] dithiophene unit. *Dyes and Pigments*. 2015; 115: 58–66. <https://doi.org/10.1016/j.dyepig.2014.12.012>
50. Alsoghier H., Selim M., Salman H., Rageh H.M., Santos M.A., Ibrahim S., Dongol M., Soga T., Abuelwafa A.A. NMR spectroscopic, linear and non-linear optical properties of 1,3-benzothiazol-2-yl-(phenylhydrazono)acetonitrile (BTPA) azo dye. *Journal of Molecular Structure*. 2019; 1179: 315–324. <https://doi.org/10.1016/j.molstruc.2018.11.004>
51. Najafi-Ashtiani H., Bahari A. Optical and cyclic voltammetry behavior studies on nanocomposite film of copolymer and WO<sub>3</sub> grown by electropolymerization. *Synthetic Metals*. 2016; 217: 19–28. <https://doi.org/10.1016/j.synthmet.2016.03.008>
52. Leonat L., Sbarcea G., Branzoi I. Cyclic voltammetry for energy levels estimation of organic materials. *UPB Scientific Bulletin, Series B: Chemistry and Materials Science*. 2013; 75(3): 111–118. [https://www.scientificbulletin.upb.ro/rev\\_docs\\_arhiva/ful982\\_152789.pdf](https://www.scientificbulletin.upb.ro/rev_docs_arhiva/ful982_152789.pdf)
53. Davis E.A., Mott N.F. Conduction in non-crystalline systems V. Conductivity, optical absorption and photoconductivity in amorphous semiconductors. *The Philosophical Magazine: A Journal of Theoretical Experimental and Applied Physics*. 2006; 22(179): 0903–0922. <https://doi.org/10.1080/14786437008221061>
54. Johansson T., Mammo W., Svensson M., Andersson R., Ingana O. Electrochemical bandgaps of substituted polythiophenes. *Journal of*

- Materials Chemistry*. 2003; (6): 1316–1323. <https://doi.org/10.1039/b301403g>
55. Cardona C.M., Li W., Kaifer A.E., Stockdale D., Bazan G.C. Electrochemical considerations for determining absolute frontier orbital energy levels of conjugated polymers for solar cell applications. *Advanced Materials*. 2011; 23(20): 2367–2371. <https://doi.org/10.1002/adma.201004554>
56. Ameri T., Khoram P., Min J., Brabec C.J. Organic ternary solar cells: A review. *Advanced Materials*. 2013; 25(31): 4245–4266. <https://doi.org/10.1002/adma.201300623>
57. Fariq F., Shujahadeen M., Hussein S.A. Effect of the dopant salt on the optical parameters of PVA: NaNO<sub>3</sub> solid polymer electrolyte. *Journal of Materials Science: Materials in Electronics*. 2015; 26(1): 521–529. <https://doi.org/10.1007/s10854-014-2430-0>
58. Shujahadeen B.A., Omed Gh.A., Ahang M.H., Rebar T.A., Mariwan A.R., Hameed M.A., Sarbast W.A., Awara R.M. Optical properties of pure and doped PVA: PEO based solid polymer blend electrolytes : two methods for band gap study. *Journal of Materials Science Materials in Electronics*. 2017; 28: 7473–7479. <https://doi.org/10.1007/s10854-017-6437-1>
59. Amin P.O., Kadhim A.J., Ameen M.A., Abdulwahid R.T. Structural and optical properties of thermally annealed – TiO<sub>2</sub>–SiO<sub>2</sub> binary thin films synthesized by sol-gel method. *Journal of Materials Science Materials in Electronics*. 2018; 29: 16010–16020. <https://doi.org/10.1007/s10854-018-9688-6>
60. Penzkofer A., Holzer W., Hörhold H.H. Travelling-wave lasing of TPD solutions and neat films. *Synthetic Metals*. 2000; 113(3): 281–287. [https://doi.org/10.1016/S0379-6779\(00\)00231-9](https://doi.org/10.1016/S0379-6779(00)00231-9)